Earth and Planetary Science Letters 298 (2010) 162–174

Contents lists available at ScienceDirect

Earth and Planetary Science Letters

journal homepage: www.elsevier.com/locate/epsl

A high-resolution Holocene paleomagnetic secular variation and relative paleointensity stack from eastern Canada

F. Barletta [a,b,*], G. St-Onge [a,b,c], J.S. Stoner [c,b], P. Lajeunesse [d,b], J. Locat [e]

[a] Institut des sciences de la mer de Rimouski (ISMER), 310, allée des Ursulines, Rimouski, Canada QC G5L 3A1
[b] Centre de Recherche en Géochimie et Géodynamique (GEOTOP), Box 8888, Succ. Centre-Ville, Montréal, Canada QC H3C 3P8
[c] College of Oceanic and Atmospheric Sciences, Oregon State University, 104 COAS Admin. Bldg. Corvallis, Oregon 97331-5503, USA
[d] Département de géographie & Centre d'études nordiques, Université Laval, Québec, Canada QC G1V 0A6
[e] Département de géologie et de génie géologique, Université Laval, Québec, Canada QC G1V 0A6

ARTICLE INFO

Article history:
Received 13 February 2010
Received in revised form 21 July 2010
Accepted 22 July 2010
Available online 25 August 2010

Editor: P. DeMenocal

Keywords:
Holocene
paleomagnetic secular variation stack
relative paleointensity
Laurentian Channel
eastern Canada

ABSTRACT

A high-resolution Holocene paleomagnetic secular variation (PSV) and relative paleointensity (RPI) stack was constructed using u-channel paleomagnetic data from six radiocarbon-constrained marine sedimentary sequences raised along the main axis of the Laurentian Channel (eastern Canada), from its head to its mouth. Centennial- to millennial-scale declination and inclination features of the eastern Canadian stack can be correlated, within the dating uncertainties, with other Holocene North American, Icelandic and European PSV records, suggesting a common, possibly hemispheric in character, geomagnetic origin. Both magnetic inclination and declination of the eastern Canadian stack are generally consistent with the time-varying spherical harmonic model of the geomagnetic field CALS7k.2, notably during the last ~4000 cal BP. In addition, the eastern Canadian Holocene RPI stack reveals similar millennial and even centennial time-scale variations consistent with some virtual axial dipole moment (VADM) reconstructions derived from absolute paleointensity data as well as with North American lacustrine RPI records. Accordingly, these results suggest that the Holocene paleomagnetic secular variation in North America is significantly driven by large-scale (>5000 km) geomagnetic field changes at these timescales.

1. Introduction

In the last few years, a great improvement in the knowledge of the Earth magnetic field variability beyond the historical measurements (last ~400 years; e.g. Jackson et al., 2000) has been achieved. For instance, Laj et al. (2000) and Stoner et al. (2002) using high sediment accumulation-marine records from the North Atlantic and the South Atlantic respectively, have provided two high-resolution geomagnetic paleointensity stacks spanning the last ~80 kyr. However, if we focus on the Holocene period, much of the paleomagnetic secular variation (PSV) records was mainly derived from Northern Hemisphere continental lake sediments and full-vector reconstructions using stacked data from sedimentary sequences are still rare (e.g., Turner and Thompson, 1981; Stockhausen, 1998; King and Peck, 2001; Snowball et al., 2007). Combining paleomagnetic data from many PSV records has the advantage of reducing local lithological effects thus enhancing the true geomagnetic signal.

In addition, because the geomagnetic dipole moment affects the local cosmic ray cutoff rigidity (e.g., Elsasser et al., 1956) understanding the temporal variability of the geomagnetic field behaviour is a key factor to infer past solar activity (e.g., Solanki et al., 2004; Usoskin et al., 2006), as well as the long-term behaviour of the solar dynamo (Usoskin et al., 2007) derived from cosmogenic isotopes (^{14}C and ^{10}Be) in natural archives. On the other hand, using physics-based models, Kovaltsov and Usoskin (2007) and Usoskin et al. (2008) also highlighted the concomitant role of centennial geomagnetic and solar activity changes in affecting the regional tropospheric ionization, which provides new insights about the effect of cosmic rays on climate (e.g., Usoskin and Kovaltsov, 2008). However, one of the major sources of incertitude in these physics-based models is an incomplete knowledge of how geomagnetic field varied in the past (e.g., Snowball and Muscheler, 2007).

In this paper, we provide the first eastern Canadian radiocarbon-constrained Holocene paleomagnetic secular variation (PSV) and relative paleointensity (RPI) stack derived from six marine sedimentary sequences raised from the head to the mouth of the Laurentian Channel. The quality and the accuracy of the stack are tested by comparing our record with other high-resolution Holocene Northern Hemisphere PSV and RPI records as well as the CALS7k.2 time-varying spherical harmonic model of the geomagnetic field (Korte et al., 2005). Lastly, we assess the North American geomagnetic field behaviour throughout the Holocene.

* Corresponding author. Tel.: +1 418 723 1986x1230; fax: +1 418 724 1842.
E-mail address: francesco.barletta@uqar.qc.ca (F. Barletta).

0012-821X/$ – see front matter © 2010 Elsevier B.V. All rights reserved.
doi:10.1016/j.epsl.2010.07.038

2. Geological setting

2.1. Stratigraphy and sedimentology

Piston cores MD99-2220, COR0602-36PC and COR0602-42PC (hereinafter 36PC and 42PC) were collected in the Lower St. Lawrence Estuary, whereas cores COR0503-CL03-35PC, COR0503-CL04-36PC and COR0503-CL05-37PC (hereinafter 35PC, CL04-36PC and 37PC) in the Gulf of St. Lawrence (Fig. 1; Supplementary materials, Table 1). Since the late 1970s, the Late Quaternary marine geology of the region was investigated by many authors using geophysical data principally derived from high-resolution seismic-reflection profiles (e.g., Syvitski and Praeg, 1989; Josenhans and Lehman, 1999; Duchesne et al., 2007; St-Onge et al., 2008; Duchesne et al., 2010), and by coring (e.g., Keigwin and Jones, 1995; Josenhans and Lehman, 1999; St-Onge et al., 2003; Cauchon-Voyer et al., 2008; St-Onge et al., 2008). Five major stratigraphic units associated with the retreat of the Late Wisconsinan Ice Sheet and the establishment of postglacial conditions was recognised by Syvitski and Praeg (1989) in the St. Lawrence Estuary. From the base to the top, these units were interpreted as: Unit 1, till or ice-contact sediments deposited by grounded glacial ice; Unit 2, ice-proximal, coarse-grained glaciomarine sediments deposited either during the rapid retreat of an ice terminus or in an ice-front stillstand setting; Unit 3, ice-distal, fine-grained glaciomarine sediments correlated to the Goldthwait Sea clays (Dredge, 1983) mapped onshore; Unit 4, paraglacial deltaic sediments; and Unit 5, postglacial sediments deposited under modern oceanographic conditions. Based on detailed rock magnetic and sedimentological analyses performed on a long piston core (~51 m; core MD99-2220 utilized in this study) retrieved from the Lower St. Lawrence Estuary, St-Onge et al. (2003) confirmed the presence of Units 3 and 5 reported by Syvitski and Praeg (1989), whereas St-Onge et al. (2008) cored and dated the ice-proximal glaciomarine unit (Unit 2 of Syvitski and Praeg 1989). Furthermore, during the last ~8500 cal BP, the mean sedimentation rate of core MD99-2220 was estimated to vary between ~1.2 and 4.2 m/kyr, whereas older glaciomarine sediments were deposited at rates higher than ~30 m/kyr (St-Onge et al., 2003). Similarly, using high-resolution seismo-stratigraphy and piston coring within the Gulf of St. Lawrence, Josenhans and Lehman (1999) identified, from the Late Pleistocene to the Holocene, till, glaciomarine sediments and postglacial muds. Moreover, Keigwin and Jones (1995) based on earlier studies on sedimentary sequences raised from the Gulf of St. Lawrence/Scotian margin region, observed distinctive changes in lithology from red terrigenous clays, silts and sand during the glaciation to brown and gray hemipelagic sediments on deglaciation.

2.2. Holocene paleomagnetism in eastern Canada: previous studies

According to Jonkers et al. (2003), only one direct measurement of magnetic declination was made offshore before 1590 AD northeast of

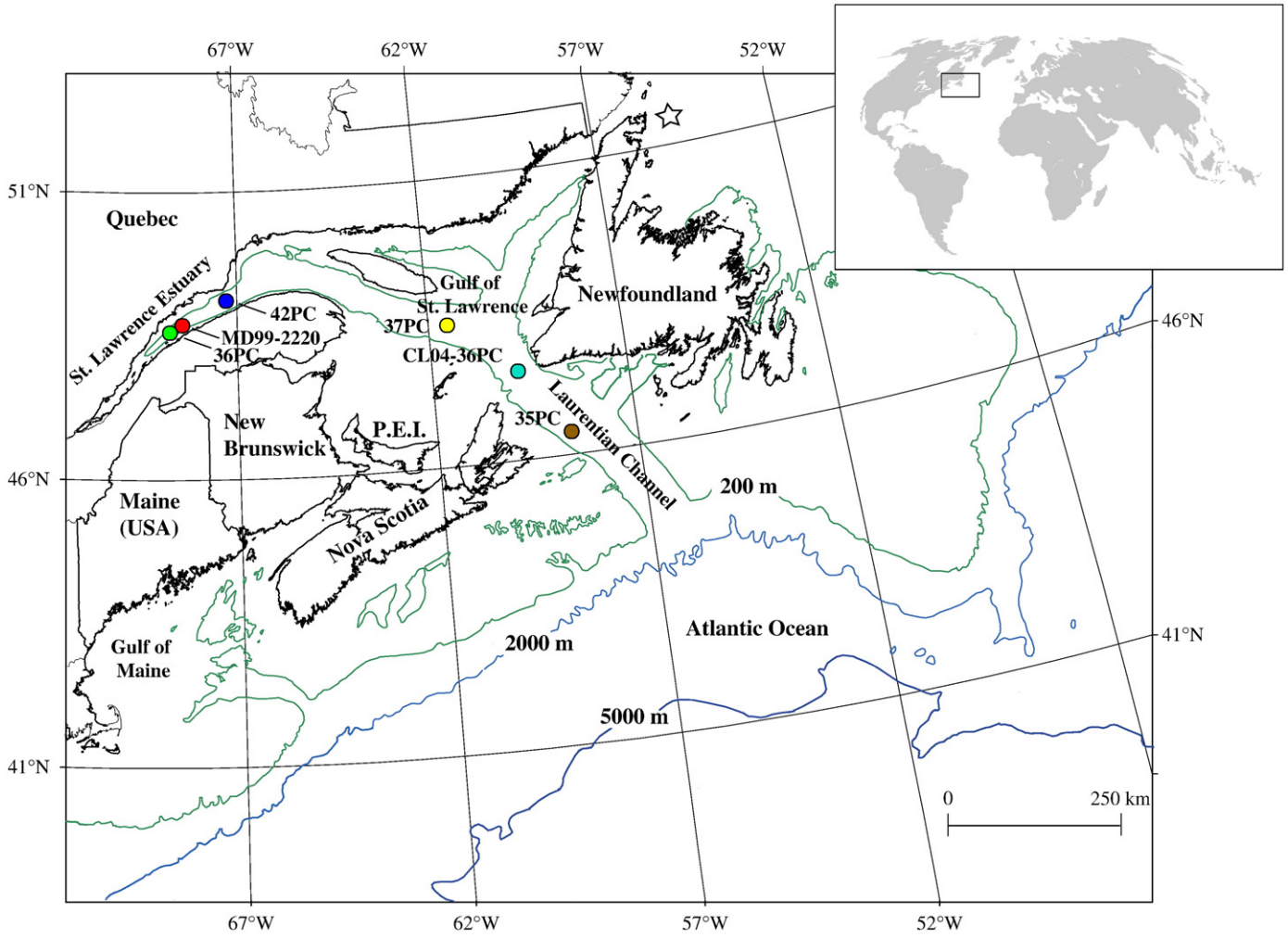

Fig. 1. Map of eastern Canada and location of the piston cores. The box in the inset shows the location of the study area whereas the open star indicates the first historical reading of magnetic declination made before 1590 AD according to Jonkers et al. (2003). Bathymetric contours at 200, 2000 and 5000 m, are also indicated. Modified from Shaw et al. (2002). P.E.I. = Prince Edward Island.

Newfoundland (Fig. 1). Subsequently direct readings of the geomagnetic components (mainly magnetic declination) were made by European mariners in the Nova Scotia and Newfoundland margin area since 1590 AD. Apart from these historical measurements, a detailed paleomagnetic study (spanning the last ~8500 cal BP) from the St. Lawrence Estuary was conducted by St-Onge et al. (2003). This study revealed that the postglacial sediments from the St. Lawrence Estuary (core MD99-2220) preserved a millennial and even centennial timescale reliable PSV and relative paleointensity (RPI) record. Other previous Holocene PSV studies come mainly from northern American continental lakes, notably: Fish Lake (Oregon, USA; Verosub et al., 1986), Lake St. Croix (Minnesota, USA; Lund and Banerjee, 1985), Lake Pepin (Minnesota, USA; Brachfeld and Banerjee, 2000) and the eastern US stack (obtained by combining PSV from three eastern North American lakes: Seneca Lake (New York), Lake LeBoeuf (Pennsylvania) and Sandy Lake (Pennsylvania); King and Peck, 2001). In addition, Hagstrum and Champion (2002) provided a Late Pleistocene to Holocene PSV record using ^{14}C-dated volcanic rocks from western North America.

3. Sampling and methods

Core MD99-2220 was collected during the IMAGES-V (International Marine Past Global Change Study) oceanographic campaign, in July 1999, on board the *Marion Dufresne II*, whereas all the other piston cores (PC) were collected on board the R/V *Coriolis II* during two different cruises in June 2005 (COR0503) and 2006 (COR0602) respectively. The details of the methodology, as well as the results of core MD99-2220 utilized in this study are exhaustively described in St-Onge et al. (2003) and will not be further discussed.

On board the R/V *Coriolis II*, cores CL04-36PC, 35PC, 36PC, 37PC and 42PC were recovered using a modified version of a Benthos^{TM} piston corer, allowing the sampling of cores up to 7.90 m. All coring sites were targeted using high-resolution seismic profiles indicating high sediment accumulation areas not influenced by turbidites or other mass wasting events.

3.1. Multisensor core logger

On board, the cores were run into a GEOTEK Multisensor Core Logger (MSCL; e.g., St-Onge et al., 2007) for the determination of wet bulk density by gamma ray (γ) attenuation and volumetric magnetic susceptibility (k_{LF}). Both measurements were performed at 1 cm intervals. The values of k_{LF} primarily reflect changes in the ferrimagnetic concentration (e.g., magnetite or titanomagnetite), but are also sensitive to grain size variations (e.g., Dunlop and Özdemir, 1997). The γ-ray attenuation values, after proper calibration procedure, provide the wet bulk density of the sediment (St-Onge et al., 2007).

3.2. Diffuse spectral reflectance

Diffuse spectral reflectance (sediment colour) data were acquired at 5 cm intervals using an X-Rite DTP22 hand-held spectrophotometer immediately after splitting the cores. Subsequently, the data were converted into the CIE (*Commission Internationale de l'Éclairage*/International Commission on Illumination) L* a* b* (L*, lightness; a*, from green to red; b*, from blue to yellow) colour space. In paleomagnetism, a* can be a useful parameter to detect variations in high-coercivity red minerals such as hematite (e.g., St-Onge et al., 2007).

3.3. Grain size

All grain size analyses were performed using a Beckman-Coulter LS-13320 (0.04 to 2000 μm) laser diffraction analyzer at 10 cm intervals. About 2 g of wet sediment was mixed in a solution of 20 g L^{-1} of Calgon electrolytic solution (sodium hexametaphosphate) and water. The samples were rotated for at least 3 h using an in-house rotator and then sieved over the instrument (2 mm) prior to analysis. All the particle size distributions output were then processed using the Gradistat software (Blott and Pye, 2001). An average of at least two measurements was used for the calculations.

3.4. Magnetic remanence analyses

The natural remanent magnetization (NRM) was measured on u-channel samples using a high-resolution cryogenic magnetometer (2G Enterprises Model SRM-755) at 1 cm intervals. In order to isolate the characteristic remanent magnetization (ChRM), the NRM was measured and progressively demagnetized using stepwise peak alternating fields (AF) up to 70 mT in 5 mT steps. Magnetic declination (Dec) and inclination (Inc) of the ChRM (labelled as ChRM Dec and ChRM Inc, respectively) were calculated at 1 cm intervals using the standard principal component analysis (PCA) of Kirschvink (1980). Since the cores were not azimuthally oriented, the ChRM Dec profiles are relative. The precision of the best-fit procedure was estimated by the maximum angular deviation (MAD; Kirschvink, 1980). In the context of PSV and RPI studies of Quaternary marine sediments, MAD values below 5° are often considered as high quality data (Stoner and St-Onge, 2007).

An anhysteretic remanent magnetization (ARM) was imparted using a 100 mT AF field with a 50 μT direct current (DC) biasing field. The ARM was measured following progressive AF demagnetization up to 50 mT with steps every 5 mT. The ARM was also expressed as anhysteretic susceptibility (k_{ARM}) by normalizing the ARM with the biasing field. The k_{ARM} versus k_{LF} diagram was used to assess the extent and uniformity of the magnetic grain size distribution (King et al., 1983). An isothermal remanent magnetization (IRM) was imparted to the z axis of the u-channels with a DC pulse field of 0.3 T using a 2G Enterprises pulse magnetizer. The IRM was then demagnetized as the same AF steps of the ARM. Lastly, the median destructive fields of the NRM, ARM and IRM (labelled as MDF_{NRM}, MDF_{ARM} and MDF_{IRM}, respectively; i.e., the value of the peak AF necessary to reduce the magnetic remanence to half of its initial value) were calculated using the software developed by Mazaud (2005). In the case of single NRM component, the MDF_{NRM} reflects the mean coercivity state of the magnetic grain assemblage which in turn depends on both the grain size and mineralogy (e.g., Dunlop and Özdemir, 1997). Furthermore, if the magnetic mineralogy is mainly controlled by single domain (SD)/pseudo single domain (PSD) magnetite, the MDF_{IRM} are lower than MDF_{ARM} values (Dunlop and Özdemir, 1997). Accordingly, the use of these three parameters provides some indications concerning magnetic mineralogy and grain size variations.

3.5. Hysteresis properties and IRM acquisition curves

Hysteresis properties were measured using an alternating gradient magnetometer (AGM) MicroMag 2900 from Princeton Measurements Corporation on some pilot samples at intervals with important changes in the diffuse spectral reflectance measurements (a* profiles). Hysteresis loops along with backfield remanence curves were used to determine saturation magnetization (Ms), coercive force (Hc), saturation remanence (Mrs) and coercivity of remanence (Hcr). The ratios Mrs/Ms and Hcr/Hc can be used as grain size proxies (the so-called Day plot) as well as to identify the magnetic domain state when the principal remanence-carrier mineral is magnetite (Day et al., 1977). Lastly, a stepwise IRM acquisition was conducted on the AGM applying a magnetic induction field up to ~1 T. This type of experiment is useful to determine the range of coercivities over which significant acquisition occurs (e.g., Jackson, 2007).

3.6. Radiocarbon dating

The chronology of each core was determined using AMS-^{14}C measurements on marine shell fragments for a total of 28 dates (Supplementary materials, Table 2). All radiocarbon ages were calculated using Libby's half-life and corrected for natural and sputtering fractionation ($\delta^{13}C = -25‰$ versus Vienna Pee-Dee Belemnite (VPDB)) following the convention of Stuiver and Polach (1977). The conventional ^{14}C ages were then calibrated using the online CALIB 5.0.2 software (Stuiver et al., 2005) and the Hughen et al. (2004) marine dataset. A standard marine reservoir correction of ~400 years ($\Delta R = 0$) to account for the apparent age of dissolved inorganic carbon in high-latitude North Atlantic waters was applied to all dates (Bard, 1998). The chronology of each core is presented only between the uppermost and lowermost radiocarbon dates.

4. Results

4.1. Stratigraphy

As revealed from grain size measurements, the overall trend in the mean grain size of all cores appears quite similar (Fig. 2). As a whole, the sediments of all cores consist of two distinct sedimentary units. The upper unit is composed of dark gray, bioturbated silty clays to sandy mud, whereas the lower unit is composed of lighter gray and relatively homogenous, slightly bioturbated to massive clayey silts to silty clays (Fig. 2). According to the previous studies of Josenhans and Lehman (1999) and St-Onge et al. (2003), the lowermost and the uppermost units were interpreted as glaciomarine and postglacial sediments, respectively. As depicted from Fig. 2, the transition from the two units is sharp (see also St-Onge and Long 2009), and seems synchronous and clearly evident along the West–East coring transect, suggesting a possible common origin. As already pointed out by St-Onge et al. (2003), the best candidate to explain this transition could be the re-rerouting of the Laurentide Ice Sheet meltwaters through Hudson Bay and Strait following the catastrophic drainage of the glacial Lake Agassiz-Ojibway at ~8470 cal BP (e.g., Barber et al., 1999; Lajeunesse and St-Onge, 2008).

4.2. Chronology

Five age models were constructed using the available calibrated ages on a composite depth-scale corrected for the missing sediment due to the piston coring process (Supplementary materials, Fig. A). Apart from 42PC, where a linear fit was used ($R = 0.998$), a third degree polynomial fit was utilized for cores 36PC ($R = 0.994$) and 35PC ($R = 1$) whereas an interpolation function was used for cores CL04-36PC and 37PC (Fig. 3). An abrupt change in the mean sedimentation rate of core 37PC from ~190 to ~40 cm/kyr is observed, at around 8500 cal BP. An important change in sedimentation rates is also observed in core MD99-2220 (St-Onge et al., 2003) and was previously associated with an important reduction in sediment inputs following the re-routing of the Laurentide Ice Sheet meltwaters from the St. Lawrence Estuary to the Hudson Bay and Strait after the outburst flood of Lake Agassiz-Ojibway. Unfortunately, the dating of core 36PC and 42PC does not go far back in time to see that transition, whereas in the two cores located at the most seaward locations and possibly due to the scarcity of dated material prior to ~8500 cal BP, no drastic changes in the sedimentation rates are apparent throughout the Holocene.

4.3. Magnetic mineralogy and grain size

As revealed by the k_{ARM} versus k_{LF} diagrams (Supplementary materials, Fig. B; King et al., 1983), magnetic granulometry of cores 36PC and 42PC are compatible with the presence of magnetite in the ~1–5 and ~0.1–15 μm grain size ranges, respectively. In contrast, magnetite grain size of cores 35PC, CL04-36PC and 37PC is comprised between 1 and ~15 μm. Both hysteresis loops and IRM acquisition curves indicate saturation fields below ~150 mT and coercivities typical of magnetite (e.g., Dunlop and Özdemir, 1997; Supplementary materials, Fig. C). However, an applied field of ~600 mT was necessary to saturate the sample at 758 cm of core 37PC indicating also the presence of a high-coercivity magnetic mineral (Supplementary materials, Fig. C). On the other hand, the MDF_{NRM} and MDF_{ARM} values range between 25 and ~30 mT for all cores whereas the MDF_{IRM} values are lower (Supplementary materials, Fig. D). These values are compatible with the presence of magnetite as the dominant ferrimagnetic mineral. According to the Day plot, much of the pilot samples (selected in intervals of apparent lithological changes) fall in the coarse end of the PSD region (Supplementary material, Fig. E). However, some data points are not comprised in the usual SD/MD mixing line implying either a different magnetic state domain distribution or a more complex magnetic mineralogy (or both). Theoretical calculations show that a mixture of SD/MD and superparamagnetic (SP) particles (the maximum size for SP behaviour is generally taken to be ~30 nm; Dunlop, 1973) with increasing grain size tends to increase the Hcr/Hc ratio outside the usual PSD region for synthetic magnetite (e.g., Krása and Fabian 2007 and references therein).

4.4. Paleomagnetism

For all cores, a stable, well-defined paleomagnetic direction was isolated by PCA analysis (Kirschvink, 1980) using at least 5 consecutive AF steps at peak field between 15 and 70 mT. MAD values are almost always lower than 10° and in most of the cores lower than 5° (Fig. 4). Nevertheless, in some intervals of cores CL04-36PC and 35PC, the ChRM is not as well-defined as indicated by MAD values higher than 5°. These intervals are likely associated with a more complex magnetic mineralogy as reflected by changes in MDF and a* profiles (Supplementary materials, Figs. D and F) as well as a coarse sediments texture (Fig. 2). In addition, the upper ~150 cm of core 35PC are characterized by high-amplitude variations of the ChRM Inc. This is probably due to coring disturbance. However, apart from these intervals, all the ChRM Inc values fluctuate around the expected inclination (I_{GAD}) calculated with the geocentric axial dipole (GAD) model, (Fig. 4) thus supporting a coherent record of the PSV of the geomagnetic field.

4.5. Relative paleointensity determinations (RPI)

Estimation of relative paleointensity of the geomagnetic field in sedimentary sequences is obtained by dividing the measured NRM by an appropriate normalizer in order to compensate for the variable concentration of ferrimagnetic minerals (Tauxe, 1993). Concentration-dependent parameters such as ARM, IRM or k_{LF} are generally employed as normalizer. The use of IRM as a normalizer was successfully employed by St-Onge et al. (2003) for core MD99-2220 using the criteria proposed by Tauxe (1993) and King et al. (1983). Following the recommendations proposed by Stoner and St-Onge (2007) for Quaternary RPI studies, the NRM should be characterized by a strong, well-defined single component magnetization with MAD values <5° carried by magnetite in the ~1–15 μm (SD/PSD) grain size range (e.g., Dunlop and Özdemir, 1997). Moreover, due to the effect of magnetostatic interaction between ferrimagnetic particles on the ARM acquisition (Sugiura, 1979), concentration of magnetite should not vary downcore by more than a factor of 10 (Tauxe, 1993). As previously discussed, the magnetic mineralogy is compatible with the presence of magnetite in the PSD grain size range (Supplementary materials, Fig. B). Furthermore, the ChRM is also well-defined

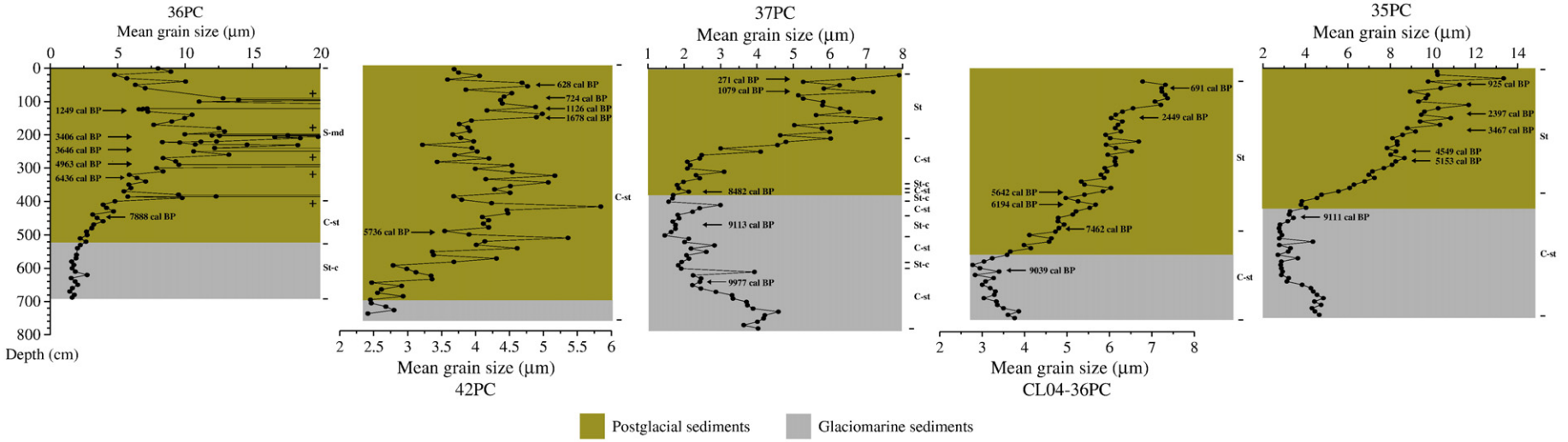

Fig. 2. Mean grain size versus depth. Also illustrated are the calibrated ages (see text for details). Glaciomarine and postglacial sediments are indicated with the gray and olive area, respectively. The grain size data were computed using the Gradistat software (Blott and Pye, 2001). The sediment texture is indicated on the right of each diagram. St-c = Silty clays; C-st = Clayey silts; St = Silts; S-md = Sandy muds.

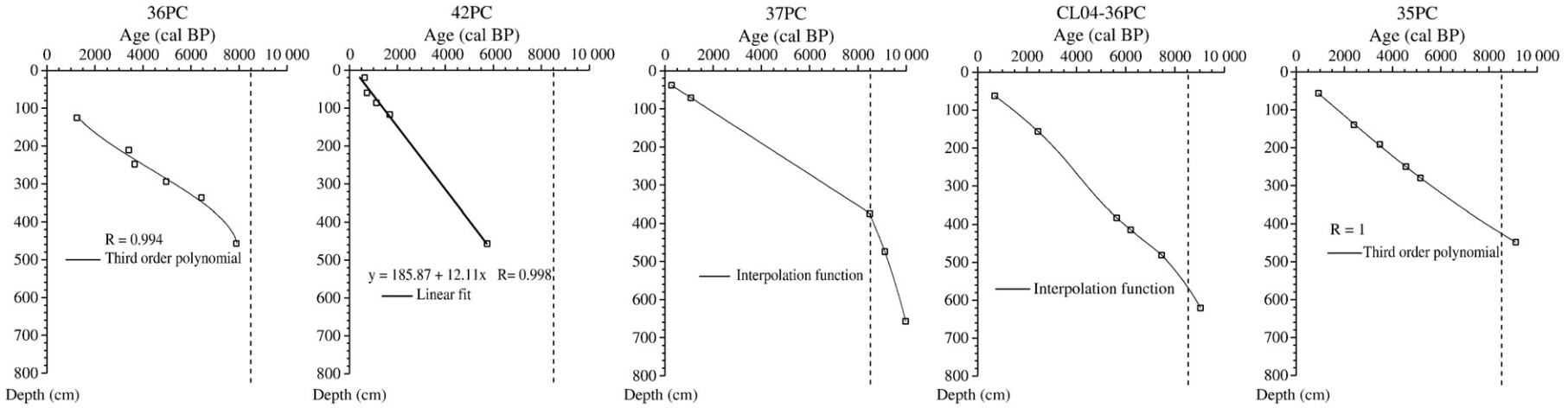

Fig. 3. Age models. The vertical dashed line depicts the important change in the sedimentation rates observed in cores 37PC and MD99-2220 from the Lower St. Lawrence Estuary at ~8500 cal BP (see text for details).

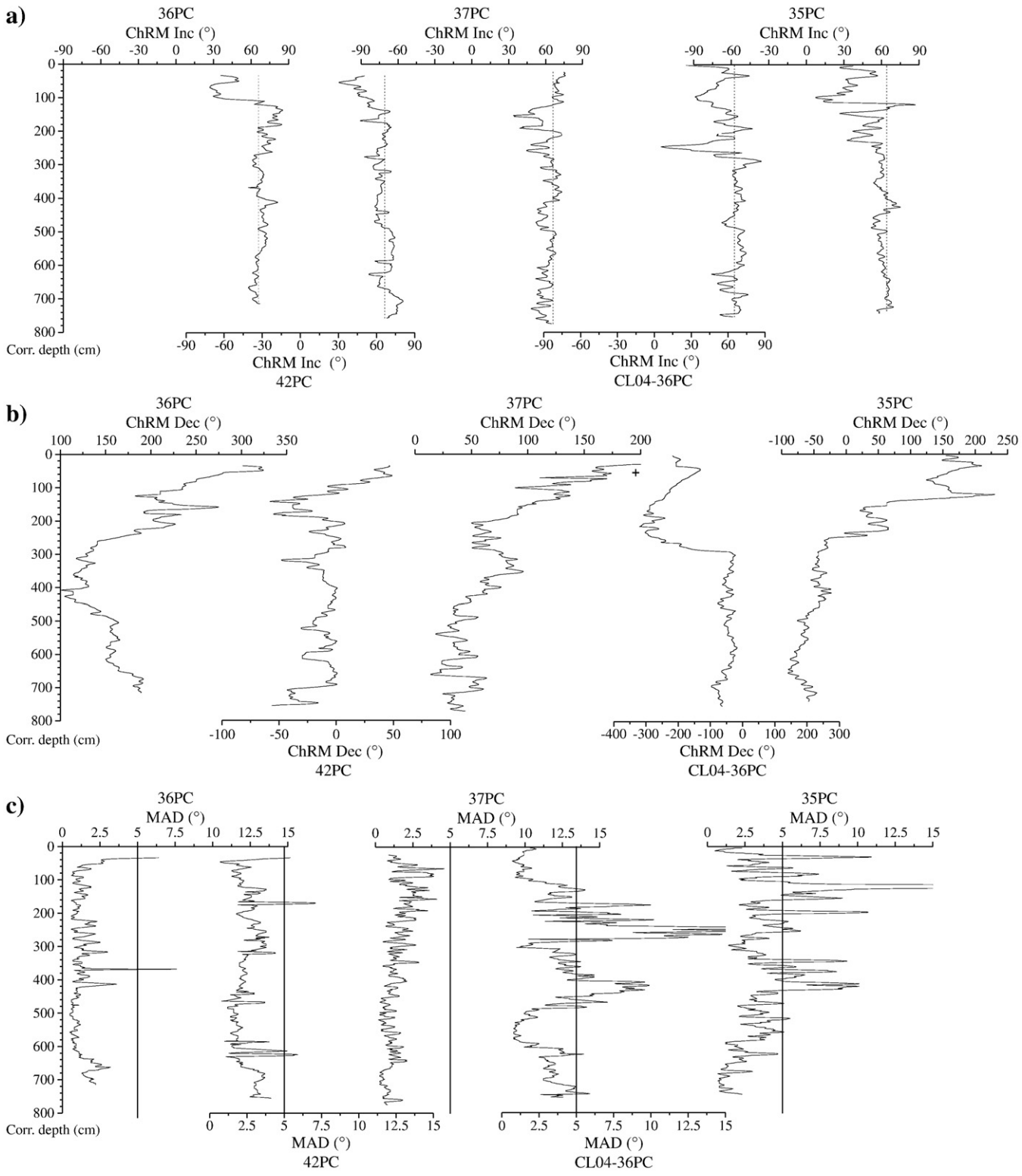

Fig. 4. Characteristic remanent magnetization (ChRM) declination (Dec) and inclination (Inc) as well as the corresponding maximum angular deviation (MAD) values (the vertical solid line in the MAD diagrams is the 5°). The broken vertical lines in the ChRM Inc diagrams represent the expected magnetic inclination (I_{GAD}) according to a geocentric axial dipole (GAD) model. Note that the ChRM Dec values are relative.

(MAD<10°; Fig. 4) whereas the low-field magnetic susceptibility varies within a factor of 10 (Supplementary materials, Fig. F).

The choice for the appropriate normalizer can be discussed in several ways (see review of Valet, 2003). Levi and Banerjee (1976) suggested using the remanence whose demagnetization curve most closely resembles that of NRM. This can be assessed by comparing the AF coercivity spectra of the NRM, ARM and IRM. As depicted from Fig. G, Supplementary materials (left diagrams) coercivity spectra of the ARM and NRM are nearly identical in the selected coercivity windows (shaded regions) while that of the IRM is much softer. Furthermore, the ratio of NRM/IRM (and hence the assumed paleointensity) is more sensitive to the AF field used for demagnetization than the NRM/ARM

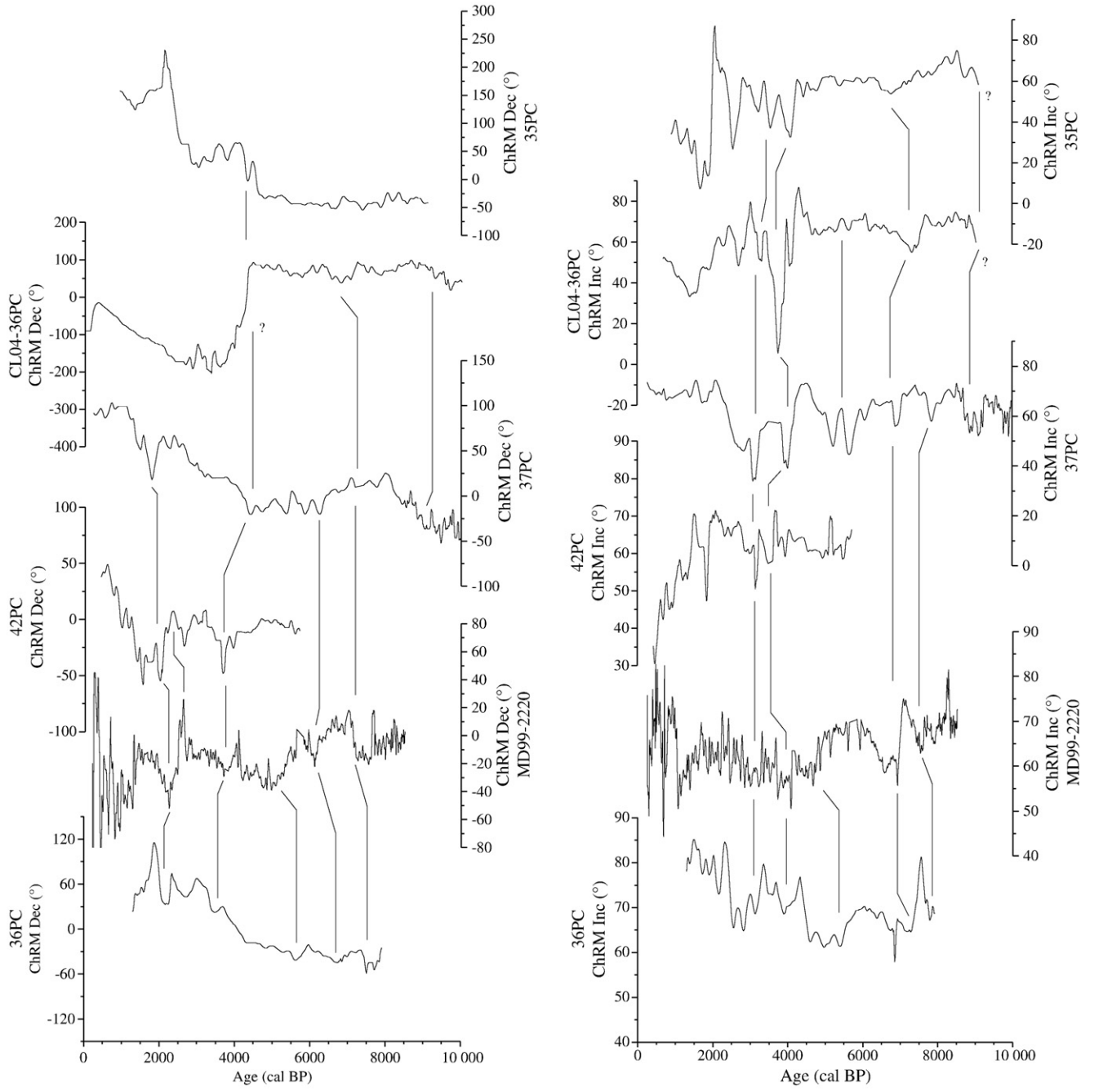

Fig. 5. Declination (left diagrams) and inclination (right diagrams) profiles for the six sedimentary sequences on their own chronologies. Some correlative magnetic features are indicated.

ratio (Supplementary materials, Fig. G; right diagrams). Based on these results, the ARM activates the same magnetic assemblages carried by the NRM and therefore is the preferred normalizer for all cores. Lastly, to construct the RPI proxies, we calculate the average of the NRM/ARM ratio over the 20–30 mT AF range and then divided each mean by the standard deviation.

4.6. Holocene full-vector magnetic master curve for eastern Canada

4.6.1. Paleomagnetic data distribution

Two frequency histograms were constructed for the paleomagnetic direction and RPI stacks according to bins of 500 years (Supplementary materials, Fig. H). The sample population for the directional and RPI data are 3441 and 3422, respectively. During the period between 8500 and 8000 cal BP, a maximum in the number of data points is observed (~260). As discussed in the previous section, this period corresponds to an important increase in sediment accumulation rate. In contrast, in the period earlier than 9000 cal BP and after 500 cal BP the number of data points does not exceed 100 due to coring disturbance in the uppermost part of the records and the limited ^{14}C ages in each individual record.

4.6.2. Construction of the stack

Because changes in the ChRM Dec profile of each core and the ones from previously published papers are relative, the ChRM Dec of each sedimentary sequence was initially standardized by subtracting from each ChRM Dec value the arithmetic mean and then dividing by the standard deviation. All these new variables are thus characterized by

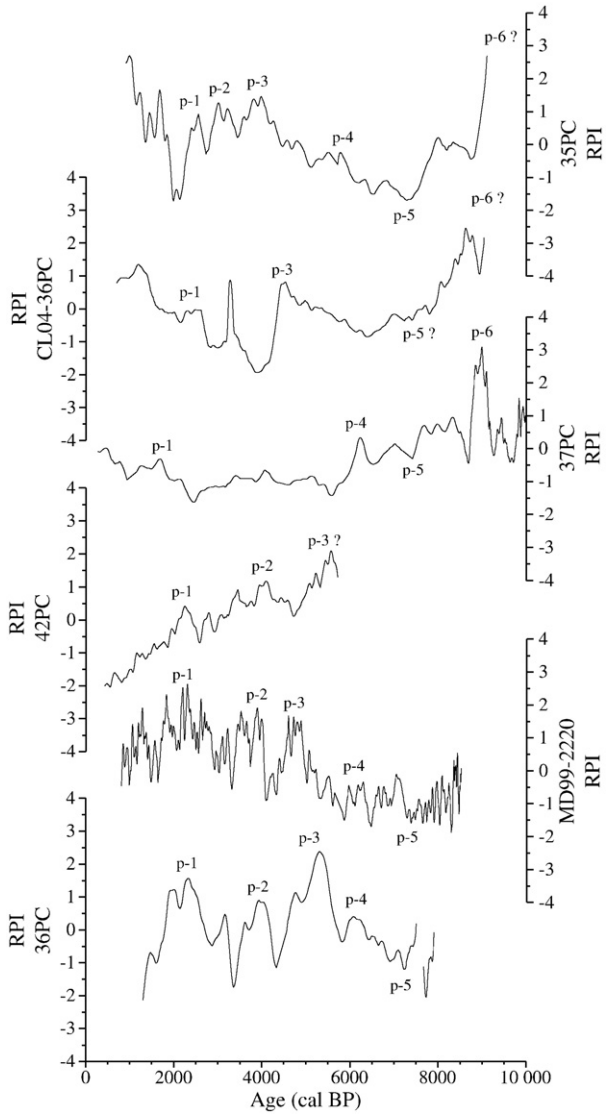

Fig. 6. Relative paleointensity (RPI) records for all cores displayed on their own chronology. Correlative paleointensity features are indicated (p-1 to p-6).

an arithmetic mean of zero and a standard deviation of 1. The same procedure was performed for the RPI records. In contrast, no treatment was necessary for the ChRM Inc as the values are absolute and vary between 0° and 90°. Subsequently, all the records were combined according to their own chronology. As revealed from Figs. 5 and 6, similar magnetic directional and relative paleointensity features can be easily detected among the records suggesting the geomagnetic field as the principal source of these variations. Nevertheless, some discrepancies are observed in the amplitude of the PSV and RPI individual records. Differences in the amplitude of these records can originate from true changes in geomagnetic field, different sedimentation rates (Fig. 3), lock-in processes as well as the nature of the sediment (Fig. 2). Other possible non-magnetic causes of variation can be ascribed to sediment coring artefacts, sediment deformation and analytical errors. Furthermore, another source of incertitude reflected in the offset between the peaks and the troughs is associated with the chronology of each individual record. Accordingly, some smoothing of the data is needed to enhance the signal/noise ratio (i.e. geomagnetic signal versus local environmental effects). A 20-point smoothing was applied to all data in order to reduce the high-frequency scatter. Subsequently, upper and lower 95% confidence limits associated to each smoothed value (X) were calculated using the formula

$$\textit{Upper (lower) limit } 95\% = X \pm \left(SEM \bullet 1.96\right),$$

where SEM is the standard error of the mean and 1.96 is the approximate value of the 0.975 quantile of the normal distribution (e.g.,Taylor, 1997).

5. Discussion

5.1. Holocene Northern Hemisphere paleomagnetic secular variation comparison

Fig. 7 shows the magnetic declination and inclination profiles of the eastern Canadian stack along with North American PSV records from Fish Lake (Oregon, USA; Verosub et al., 1986), Lake St. Croix (Minnesota, USA; Lund and Banerjee, 1985), Lake Pepin (Minnesota, USA; Brachfeld and Banerjee, 2000), the eastern US stack (King and Peck, 2001) and the PSV record from lava flows (western North America; Hagstrum and Champion, 2002). In order to assess the spatial extent of the PSV features, the Icelandic (Stoner et al., 2007) and the Fennoscandian stack records (Snowball et al., 2007) are also displayed. As observed from Fig. 7, a large number of magnetic declination and inclination features can be easily correlated within the North American and even in the European regions suggesting that such directional patterns are likely hemispheric in scale. Notably, a large magnetic declination swing is observed at ~2500 cal BP in all records. This magnetic feature ("f-event") was previously noted in Northern lacustrine European PSV records by Turner and Thompson (1981) and more recently it has also been observed in two other PSV records from Icelandic lakes (Olafsdottir et al., 2009). The different nature of these records (marine, lacustrine and volcanic) further corroborates the geomagnetic origin of these records. However, as already discussed by St-Onge et al. (2003), much of the temporal offset observed among the North American PSV records could be ascribed to the dating technique, lock-in processes as well as incertitude in the age models used. Furthermore, the main problem with radiocarbon dating of bulk carbon from lacustrine sediment is the contamination by "old" carbon. For instance, for the Lake St. Croix (Lund and Banerjee, 1985) and in the construction of the eastern US stack (King and Peck, 2001) records, the authors systematically corrected each radiocarbon date for "old" carbon contamination assuming that the same correction was valid throughout the Holocene. The same potential chronological offset could be found in the Lake Pepin record, where the chronology was partially obtained after paleomagnetic correlation with the Lake St. Croix record. In addition, "old" carbon contamination was also evocated by Hagstrum and Champion (2002) to explain the ~280 years offset observed between the Fish Lake and lava flows records for the last ~3500 years BP. Similarly, even if marine carbonates dated with the AMS-^{14}C dating method are not affected by this problem, an unknown (and variable) reservoir age effect could lead to an error in the age determination. Based on these considerations, all the proposed correlations are most likely within dating uncertainties and not different in their timing.

5.2. Eastern Canada PSV stack versus the CALS7k.2 model

As observed from Fig. 8, a general agreement is found between the eastern Canadian PSV stack and the time-varying spherical harmonic model of the geomagnetic field CALS7k.2 (Korte et al., 2005). Much of the directional features detected in Fig. 8 is well reproduced in the CALS7k.2 model, notably for the last ~4000 cal BP. The "f-event" is also well reproduced. Despite the limitation due to both the time

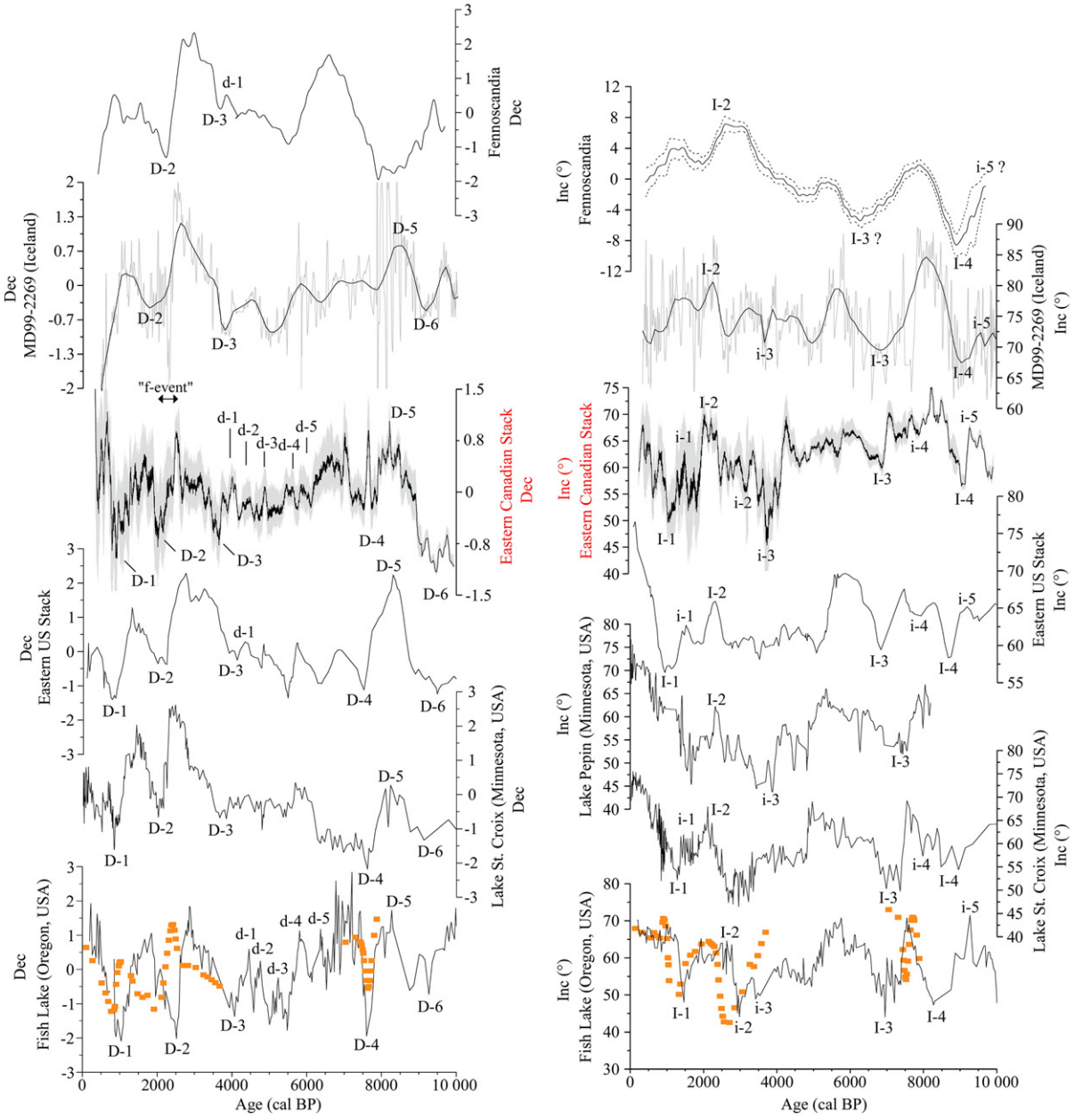

Fig. 7. Comparison of Holocene PSV records from the Northern Hemisphere. Declination (left diagrams) and inclination (right diagrams) profiles of the eastern Canadian stack compared with the Fish Lake (Oregon, USA; Verosub et al., 1986), Lake St. Croix (Minnesota, USA; Lund and Banerjee, 1985), Lake Pepin (Minnesota, USA; Brachfeld and Banerjee, 2000), eastern US stack (King and Peck, 2001) and the PSV from lava flows records (orange squares in the web version; Hagstrum and Champion, 2002). The PSV Icelandic and Fennoscandian stack are from Stoner et al. (2007) and Snowball et al. (2007), respectively. The black curve in the Icelandic record is a weighted function applied to the raw data (gray curve in the web version) whereas the dotted curves in the relative inclination record from Fennoscandia are 95% confidence limits. The Fish Lake data were calibrated using the Stuiver et al. (1998) radiocarbon calibration curve (K. Verosub, personal communication, 2008). Lakes St. Croix, Pepin and the eastern US stack records were calibrated using the atmospheric data from Reimer et al. (2004). Proposed correlative declination and inclination features are indicated. The magnetic declination swing at ~2500 cal BP is labelled as the "f-event" (see text for details). The black curve in the eastern Canadian stack represents a 20-point smoothing of the data whereas the light gray shaded area represents upper and lower 95% confidence limits. All the declination data were standardized to allow direct comparison. Note that the inclination scales are not identical.

resolution (~100 years) and the heterogeneous coverage of the northern American PSV database used to constrain the model, much of the northern American directional features is thus quite well reproduced by CALS7k.2.

5.3. Eastern Canadian RPI stack versus global dipole moment compilations and North American RPI records

The smoothed relative paleointensity stack from eastern Canada was compared to several global Holocene dipole moment (DM) reconstructions (Fig. 9). Apart from the synthetic record Ohno and Hamano (1993) based on a compilation of selected paleomagnetic directional data, both the recent paleointensity reconstructions of Knudsen et al. (2008) and Kovacheva et al. (2009) are based on absolute archeointensity data. The virtual axial dipole moment (VADM) spanning the last 7000 cal BP as expected from the CALS7k.2 model is also considered and illustrated in Fig. 9. As depicted from Fig. 9, the RPI record of the eastern Canadian stack reveals similar millennial-scale variations with both records of Ohno and Hamano (1993) and Knudsen et al. (2008) between ~4000 and 10000 cal BP. Interestingly, a common broad peak in the paleointensity is observed between these two DM reconstructions and the RPI

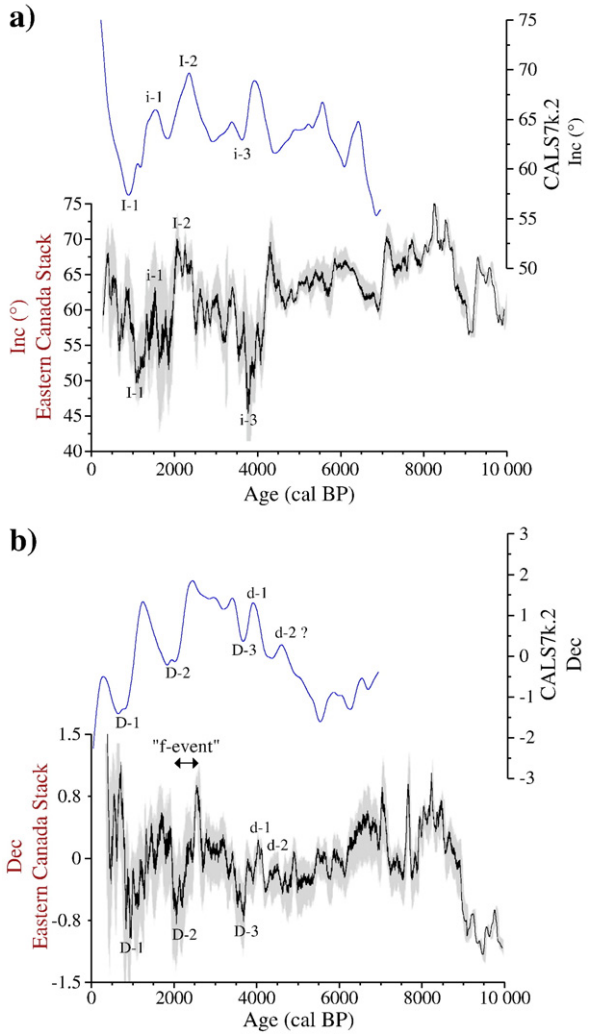

Fig. 8. Comparison between the eastern Canadian PSV stack and the CALS7k.2 model (Korte et al., 2005). (a) and (b) diagrams show the inclination (Inc) and declination (Dec) with associated 95% confidence limits (light gray shaded area), respectively. The correlative magnetic directional features illustrated are the same as labelled in Fig. 7. Note that the inclination scales are not identical.

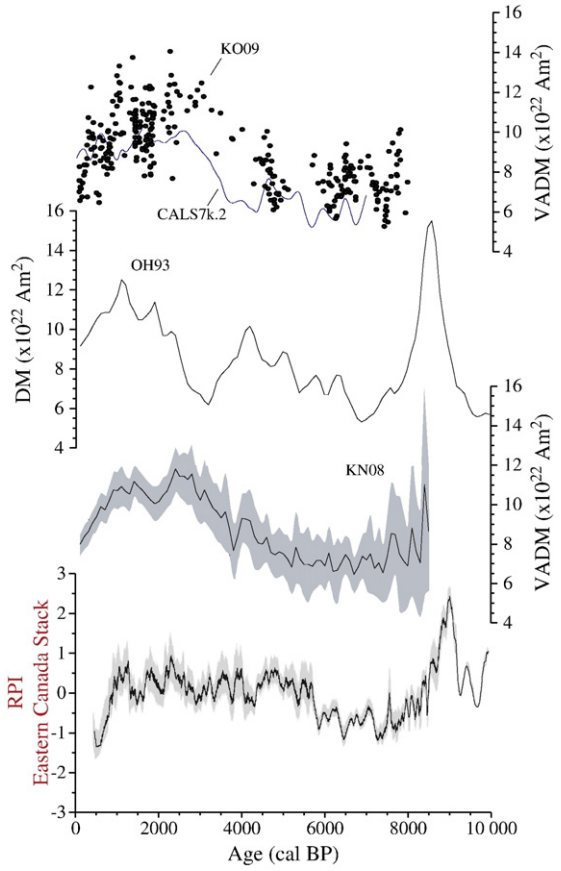

Fig. 9. Comparison of the smoothed relative paleointensity record (RPI) of the eastern Canadian stack with several dipole moment (DM) reconstructions. The light gray shaded area in the RPI record represents 95% confidence limits. KN08 and KO09 are the virtual axial dipole moment (VADM) reconstructions of Knudsen et al. (2008) and Kovacheva et al. (2009) respectively. Note that the original data from Kovacheva et al. (2009) were converted in VADM values. Here the KN08 record is considered with a 100 year time resolution. The dark gray shaded area in the KN08 record represents the 2σ uncertainties calculated using a bootstrap approach (Knudsen et al., 2008). OH93 illustrates the global DM reconstruction of Ohno and Hamano (1993). The local magnetic induction field (at the CL04-36PC core site) as expected from the CALS7k.2 model (blue curve in the web version) of Korte et al. (2005) was converted in VADM values.

stack at ~9000 cal BP. Barletta et al. (2008) already recognised this magnetic feature in a long Holocene piston core retrieved from the Chukchi Sea (Arctic Alaskan margin) and recently Snowball et al. (2010) observed an analogous paleointensity peak between 8200 and 9000 cal BP in a Holocene marine sedimentary sequence collected from the Disko Bay (Western Greenland) thus supporting a geomagnetic origin of this feature. In addition, if we focus on the period between 1000 and 4000 cal BP, a good agreement is observed between the eastern Canadian RPI stack and the other North American RPI records as well as with the VADM reconstruction of Knudsen et al. (2008) (Fig. 10). Many sub-millennial RPI features can be clearly correlated, within the dating uncertainties, among the records suggesting a common geomagnetic origin. On the other hand, the VADM values computed with the CALS7k.2 model reveal more discrepancies compared to the RPI stack both in term of fluctuation and amplitude (Fig. 10) as well as they systematically underestimate the reconstructed VADM of Knudsen et al. (2008). Korte and Constable (2005) attributed this overestimation in the reconstructed VADMs due to the presence of persistent non-dipole magnetic fields aggravated by strong regional bias in data distribution. Conversely, Knudsen et al. (2008) and Valet et al. (2008) invoked an unequal repartition of energy to higher harmonics to minimize the misfit between the inversion procedure and the data as the cause of the reduction of the global dipole moment derived from the CALS7k.2 model. However, based on the results displayed in Figs. 9 and 10 the dipole field seems to significantly drive the observed variations in the reconstructed RPI stack throughout the Holocene.

6. Conclusion

Both magnetic declination and inclination profiles of the eastern Canadian stack can be correlated with other North American PSV lacustrine and volcanic records at the millennial and even centennial time-scale during the Holocene (Fig. 7). Notably, between ~2000 and ~3500 cal BP, relative fluctuations in the declination appear coherent over ~140° of longitude in all the considered PSV records (Fig. 7). These results corroborate and extend the previous work of Lund (1996) concerning the analysis of the Holocene paleosecular variation within the North American continent. According to Lund (1996), North American PSV features appear spatially coherent over ~4000 km in the West–East direction. Moreover, based on the study of the historical secular variation, Thompson (1984) also noted a similar scale of spatial coherence. As suggested from Fig. 7, this PSV spatial scale can be further extended beyond the North American continent to Iceland and Europe. In addition, centennial- to

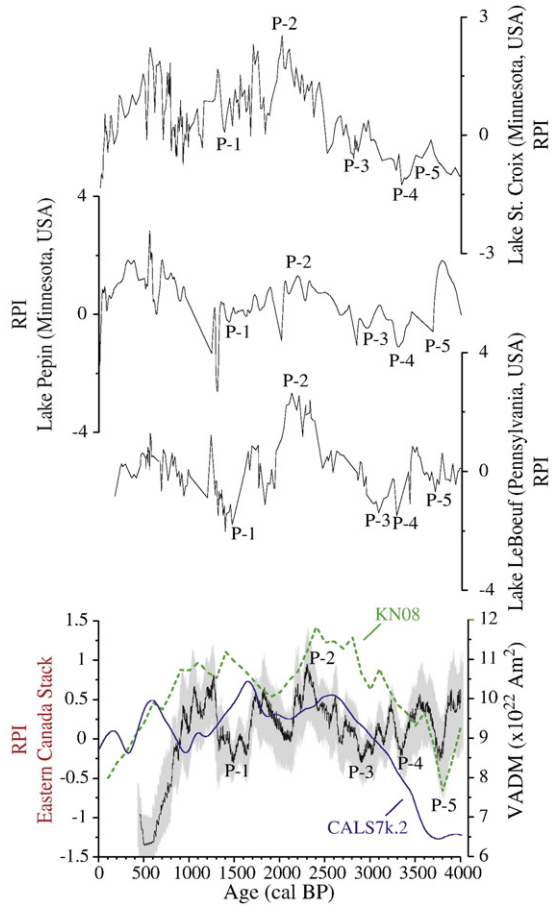

Fig. 10. Comparison of northern American RPI records spanning the last 4000 cal BP. Correlative centennial-scale RPI features are indicated (P-1 to P-5). The light gray shaded area in the RPI stack indicates 95% confidence limits. The green broken and thick blue lines represent the VADM reconstructions of Knudsen et al. (2008) and Korte et al. (2005) respectively. Note that all the RPI data are standardized for correlative purpose.

millennial-scale fluctuations of the Holocene eastern Canadian RPI stack appear coherent with the VADM reconstruction of Knudsen et al. (2008) based on absolute paleointensity data (Fig. 9) as well as with other North American lacustrine RPI records (Fig. 10) suggesting the predominance of large-scale geomagnetic field fluctuations (dipolar) in controlling the observed Holocene paleomagnetic secular variation. These results thus reveal fundamental insights about the generation of the Holocene geomagnetic field and from a practical point of view, open the possibility of using the eastern Canadian PSV and RPI stacks as a chronostratigraphic tool for eastern North America and possibly for the rest of Canada and the United States.

Acknowledgements

We wish to thank the captain, officers, crew and scientists on board the R/V *Coriolis II* for the successful recovery of the cores from the COR0503 and COR0602 expeditions. We also thank two anonymous reviewers, Dr. Leonardo Sagnotti (INGV) and Dr. Vadim A. Kravchinsky for their thorough reviews and helpful comments as well as Dr. M. Korte for providing the CALS7k.2 model outputs. Finally, we wish to thank Sylvain Leblanc and Mélanie Simard for the grain size measurements as well as Jacques Labrie for Matlab computations. This study was supported by NSERC (Natural Science and Engineering Research Council of Canada) through Discovery and ship time grants to G.S., J.L. and P.L. and FQRNT (Fonds québécois de recherche sur la nature et les technologies) through a New researcher grant to P.L. This is a GEOTOP contribution no. 2010-0006.

Appendix A. Supplementary data

Supplementary data associated with this article can be found, in the online version, at doi:10.1016/j.epsl.2010.07.038.

References

Barber, D.C., Dyke, A., Hillaire-Marcel, C., Jennings, A.E., Andrews, J.T., Kerwin, M.W., Bilodeau, G., McNeely, R., Southon, J., Morehead, M.D., Gagnon, J.-M., 1999. Forcing of the cold event of 8,200 years ago by catastrophic drainage of Laurentide lakes. Nature 400, 344–348.

Bard, E., 1998. Geochemical and geophysical implications of the radiocarbon calibration. Geochim. Cosmochim. Acta 62, 2025–2038.

Barletta, F., St-Onge, G., Channell, J.E.T., Rochon, A., Polyak, L., Darby, D.A., 2008. High-resolution paleomagnetic secular variation and relative paleointensity records from the western Canadian Arctic: implication for Holocene stratigraphy and geomagnetic field behaviour. Can. J. Earth Sci. 45, 1265–1281.

Blott, S.J., Pye, K., 2001. Gradistat: a grain size distribution and statistics package for the analysis of unconsolidated sediments. Earth Surf. Process. Land. 26, 1237–1248.

Brachfeld, S., Banerjee, S.K., 2000. A new high-resolution geomagnetic relative paleointensity record for the North American Holocene: a comparison of sedimentary and absolute intensity data. J. Geophys. Res. 105, 821–834.

Cauchon-Voyer, G., Locat, J., St-Onge, G., 2008. Late-Quaternary morpho-sedimentology and submarine mass movements of the Betsiamites area, Lower St. Lawrence Estuary, Quebec, Canada. Mar. Geol. 251, 233–252.

Day, R., Fuller, M., Schmidt, V.A., 1977. Hysteresis properties of titanomagnetites, grain size and compositional dependence. Phys. Earth Planet. Inter. 13, 260–267.

Dredge, L., 1983. Surficial Geology of the Sept-Îles area, Québec North Shore. Geological Survey of Canada, Memoir 408, 40 pp.

Duchesne, M., Pinet, N., Bolduc, A., Bédard, K., Lavoie, D., 2007. Seismic Stratigraphy of the Lower St. Lawrence Estuary Quaternary Deposits and Seismic Signature of the Underlying Geological Domains. Current Research 2007-D2. Geological Survey of Canada, Ottawa.

Duchesne, M.J., Pinet, N., Bédard, K., St-Onge, G., Lajeunesse, P., Campbell, C., Bolduc, A., 2010. Role of the bedrock topography in the Quaternary filling of a giant semi-enclosed basin: the Lower St. Lawrence Estuary, eastern Canada. Basin Res.. doi:10.1111/j.1365-2117.2009.00457.x.

Dunlop, D.J., 1973. Superparamagnetic and single-domain threshold sizes in magnetite. J. Geophys. Res. 78, 1780–1793.

Dunlop, D.J., Özdemir, Ö., 1997. Rock Magnetism. Cambridge University Press, Cambridge.

Elsasser, W., Ney, E.P., Winckler, J.R., 1956. Cosmic-ray intensity and geomagnetism. Nature 178, 1226–1227.

Hagstrum, J.T., Champion, D.E., 2002. A Holocene paleosecular variation record from ^{14}C-dated volcanic rocks in western North America. J. Geophys. Res. 107, 1–14.

Hughen, K.A., Baillie, M.G.L., Bard, E., Bayliss, A., Beck, J.W., Bertrand, C.J.H., et al., 2004. Marine04 marine radiocarbon age calibration, 0–26 Cal kyr BP. Radiocarbon 46, 1059–1086.

Jackson, M., 2007. Magnetization, isothermal remanent. In: Gubbins, David, Herrero-Bervera, Emilio (Eds.), Encyclopedia of Geomagnetism and Paleomagnetism. Published by Springer, Dordrecht, The Netherlands.

Jackson, A., Jonkers, A.R.T., Walker, M.R., 2000. Four centuries of geomagnetic secular variation from historical records. Philos. Trans. R. Soc. London Ser. A 358, 957–990.

Jonkers, A.R.T., Jackson, A., Murray, A., 2003. Four centuries of geomagnetic data from historical records. Rev. Geophys. 41 (2), 1006. doi:10.1029/2002RG000115.

Josenhans, H., Lehman, S., 1999. Late glacial history of the Gulf of St. Lawrence, Canada. Can. J. Earth Sci. 36, 1327–1345.

Keigwin, L.D., Jones, G.A., 1995. The marine record of deglaciation from the continental margin off Nova Scotia. Paleoceanography 10 (6), 973–985.

King, J., Peck, J., 2001. Use of paleomagnetism in studies of lake sediments. In: Last, W.M., Smol, J.P. (Eds.), Tracking Environmental Change Using Lake Sediments. Volume 1: Basin Analysis, Coring, and Chronological Techniques. Kluwer Academic Publishers, Dordrecht, The Netherlands.

King, J.W., Banerjee, S.K., Marvin, J.A., 1983. A new rock magnetic approach to selecting sediments for geomagnetic paleointensity studies: application to paleointensity for the last 4000 years. J. Geophys. Res. 88, 5911–5921.

Kirschvink, J.L., 1980. The least-squares line and plane and the analysis of paleomagnetic data. Geophys. J. R. Astron. Soc. 62, 699–718.

Knudsen, M.F., Riisager, P., Donadini, F., Snowball, I., Muscheler, R., Korhonen, K., Pesonen, L.J., 2008. Variations in the geomagnetic dipole moment during the Holocene and the past 50 kyr. Earth Planet. Sci. Lett. 272, 319–329. doi:10.1016/j.epsl.2008.04.048.

Korte, M., Constable, C., 2005. The geomagnetic dipole moment over the last 7000 years — new results from a global model. Earth Planet. Sci. Lett. 236, 348–358.

Korte, M., Genevey, A., Constable, C.G., Frank, U., Schnepp, E., 2005. Continuous geomagnetic field models for the past 7 millennia: 1. A new global data compilation. Geochem. Geophys. Geosyst. 6 (Q02H15). doi:10.1029/2004GC000800.

Kovacheva, M., Boyadziev, Y., Kostadinova-Avramova, M., Jordanova, N., Donadini, F., 2009. Updated archeomagnetic data set of the past 8 millennia from the Sofia laboratory, Bulgaria. Geochem. Geophys. Geosyst. 10, Q05002. doi:10.1029/2008GC002347.

Kovaltsov, G.A., Usoskin, I.G., 2007. Regional cosmic ray induced ionization and geomagnetic field changes. Adv. Geosci. 13, 31–35.
Krása, D., Fabian, K., 2007. Rock magnetism, hysteresis measurements. In: Gubbins, David, Herrero-Bervera, Emilio (Eds.), Encyclopedia of Geomagnetism and Paleomagnetism. Published by Springer, Dordrecht, The Netherlands.
Laj, C., Kissel, C., Mazaud, A., Channell, J.E.T., Beer, J., 2000. North Atlantic paleointensity stack since 75 ka (NAPIS-75) and the duration of the Laschamp event. Philos. Trans. R. Soc. Ser. A 358, 1009–1025.
Lajeunesse, P., St-Onge, G., 2008. Subglacial origin of Lake Agassiz–Ojibway final outburst flood. Nat. Geosci. 3, 184–188.
Levi, S., Banerjee, S.K., 1976. On the possibility of obtaining relative paleointensities from lake sediments. Earth Planet. Sci. Lett. 29, 219–226.
Lund, S.P., 1996. A comparison of paleomagnetic secular variation records from North America. J. Geophys. Res. 101, 8007–8024.
Lund, S.P., Banerjee, S.K., 1985. Late Quaternary paleomagnetic field secular variation from two Minnesota Lakes. J. Geophys. Res. 90, 803–825.
Mazaud, A., 2005. User-friendly software for vector analysis of the magnetization of long sediment cores. Geochem. Geophys. Geosyst. 6. doi:10.1029/2005GC001036.
Ohno, M., Hamano, Y., 1993. Global analysis of the geomagnetic field; time variation of the dipole moment and the geomagnetic pole in the Holocene. J. Geomagn. Geoelec. 45, 1455–1466.
Olafsdottir, S., Stoner, J.S., Geirstottir, A., 2009. High-resolution Holocene Paleomagnetic Secular Variation Records from Iceland: Marine–Terrestrial Synchronization. GSA Annual Meeting, Abstract volume.
Reimer, P.J., Baillie, M.G.L., Bard, E., Bayliss, A., Beck, J.W., Bertrand, C., Blackwell, P.G., Buck, C.E., Burr, G., Cutler, K.B., Damon, P.E., Edwards, R.L., Fairbanks, R.G., Friedrich, M., Guilderson, T.P., Hughen, K.A., Kromer, B., McCormac, F.G., Manning, S., Bronk, Ramsey, C., Reimer, R.W., Remmele, S., Southon, J.R., Stuiver, M., Talamo, S., Taylor, F.W., van der Plicht, J., Weyhenmeyer, C.E., 2004. IntCal04 Atmospheric radiocarbon age calibration, 26-0 ka BP. Radiocarbon 46, 1026–1058.
Sagnotti, L., Rochette, P., Jackson, M., Vadeboin, F., Dinarès-Turell, J., Winkler, A., Mag-Net" Science Team, 2003. Inter-laboratory calibration of low-field magnetic and anhysteretic susceptibility measurements. Phys. Earth Planet. Inter. 138, 25–38.
Shaw, J., Gareau, P., Courtney, R.C., 2002. Palaeogeography of Atlantic Canada 13–0 kyr. Quatern. Sci. Rev. 21, 1861–1878.
Snowball, I., Muscheler, R., 2007. Palaeomagnetic intensity data: an Achilles heel of solar activity reconstructions. Holocene 17 (6), 851–859.
Snowball, I., Zillén, L., Ojala, A., Saarinen, T., Sandgren, P., 2007. FENNOSTACK and FENNORPIS: Varve dated Holocene palaeomagnetic secular variation and relative palaeointensity stacks for Fennoscandia. Earth Planet. Sci. Lett. 255, 106–116.
Snowball, I., Nilsson, A., Sandgren, P., Lloyd, J., McCarthy, D., Moros, M., 2010. Holocene palaeomagnetic secular variation records and a relative palaeointensity estimate from Western Greenland (Disko Bugt). Geophys. Res. Abstr. 12 EGU2010-3422-2, EGU General Assembly.
Solanki, S.K., Usoskin, I.G., Kromer, B., Schüssler, M., Beer, J., 2004. Unusual activity of the Sun during recent decades compared to the previous 11,000 years. Nature 431, 1084–1087.
Stockhausen, H., 1998. Geomagnetic palaeosecular variation (0–13000 yr BP) as recorded in sediments from three maar lakes from the West Eifel (Germany). Geophys. J. Int. 135 (3), 898–910.
Stoner, J.S., St-Onge, G., 2007. Magnetic stratigraphy: reversals, excursions, paleointensity and secular variation. In: Hillaire-Marcel, C., de Vernal, A. (Eds.), Development in Marine Geology: Volume 1, Proxies in Late-Cenozoic Paleoceanography. Elsevier, pp. 99–138.
Stoner, J.S., Laj, C., Channell, J.E.T., Kissel, C., 2002. South Atlantic and North Atlantic geomagnetic paleointensity stacks (0–80 ka): implications for inter-hemispheric correlation. Quatern. Sci. Rev. 21, 1141–1151.
Stoner, J.S., Jennings, A., Kristjansdottir, G.B., Dunhill, G., Andrews, J.T., Hardardottir, J., 2007. A paleomagnetic approach toward refining Holocene radiocarbon based chronologies: paleoceanographic records from North Iceland (MD99-2269) and East Greenland (MD99-2322) margins. Paleoceanography 22, 1–23.
St-Onge, G., Long, B., 2009. CAT-scan analysis of sedimentary sequences: an ultrahigh-resolution paleoclimatic tool. Eng. Geol. 103, 127–133.
St-Onge, G., Stoner, J.S., Hillaire-Marcel, C., 2003. Holocene paleomagnetic records from the St. Lawrence Estuary: centennial- to millennial-scale geomagnetic modulation of cosmogenic isotopes. Earth Planet. Sci. Lett. 209, 113–130.
St-Onge, G., Mulder, T., Francus, P., Long, B., 2007. Continuous physical properties of cored marine sediments. In: Hillaire-Marcel, C., de Vernal, A. (Eds.), Proxies in Late Cenozoic Paleoceanography. Elsevier, pp. 63–98.
St-Onge, G., Lajeunesse, P., Duchesne, M.J., Gagné, H., 2008. Identification and dating of a key Late Pleistocene stratigraphic unit in the St. Lawrence Estuary and Gulf (eastern Canada). Quatern. Sci. Rev. 27, 2390–2400.
Stuiver, M., Polach, H.A., 1977. Discussion: reporting of ^{14}C data. Radiocarbon 19 (3), 355–363.
Stuiver, M., Reimer, P.J., Bard, E., Beck, J.W., Burr, G.S., Hughen, K.A., Kromer, B., McCormac, G., van der Plicht, J., Spurk, M., 1998. INTCAL98 Radiocarbon Age Calibration, 24,000–0 cal BP. Radiocarbon 40, 1041–1083.
Stuiver, M., Reimer, P.J., Reimer, R.W., 2005. CALIB 5.0. Available from http://radiocarbon.pa.qub.ac.uk/calib/.
Sugiura, N., 1979. ARM, TRM, and magnetic interactions: concentration dependence. Earth Planet. Sci. Lett. 42, 451–455.
Syvitski, J.P.M., Praeg, D.B., 1989. Quaternary sedimentation in the St. Lawrence Estuary and adjoining areas, eastern Canada: an overview based on high resolution seismo-stratigraphy. Géogr. Phys. Quatern. 43, 291–310.
Tauxe, L., 1993. Sedimentary records of relative paleointensity: theory and practice. Rev. Geophys. 31, 319–354.
Taylor, J.R., 1997. An Introduction to Error Analysis: the Study of Uncertainties in Physical Measurements. University Science Books.
Thompson, R., 1984. Geomagnetic evolution: 400 years of change on planet. Phys. Earth Planet. Inter. 36, 61–77.
Turner, G.M., Thompson, R., 1981. Lake sediment record of the geomagnetic secular variation in Britain during Holocene times. Geophys. J. R. Astron. Soc. 65 (3), 703–725.
Usoskin, I.G., Kovaltsov, G.A., 2008. Cosmic rays and climate of the Earth: possible connection. C. R. Geosci. 340, 441–450.
Usoskin, I.G., Solanki, S.K., Korte, M., 2006. Solar activity reconstructed over the last 7000 years: the influence of geomagnetic field changes. Geophys. Res. Lett. 33, L08103. doi:10.1029/2006GL025921.
Usoskin, I.G., Solanki, S.K., Kovaltsov, G.A., 2007. Grand minima and maxima of solar activity: new observational constraints. Astron. Astrophys. 471, 301–309. doi:10.1051/0004-6361:20077704.
Usoskin, I.G., Korte, M., Kovaltsov, G.A., 2008. Role of centennial geomagnetic changes in local atmospheric ionization. Geophys. Res. Lett. 35, L05811. doi:10.1029/2007GL033040.
Valet, J.-P., 2003. Time variations in geomagnetic intensity. Rev. Geophys. 41 (1), 1004. doi:10.1029/2001RG000104.
Valet, J.-P., Herrero-Bervera, E., LeMouël, J.-L., Plenier, G., 2008. Secular variation of the geomagnetic dipole during the past 2000 years. Geochem. Geophys. Geosyst. 9, Q01008. doi:10.1029/2007GC001728.
Verosub, K., Mehringer Jr., P., Waterstraat, P., 1986. Holocene secular variation in western North America: paleomagnetic record from Fish Lake, Harney County, Oregon. J. Geophys. Res. 91, 3609–3623.